A truffle-like, layer-by-layer supramolecular structure for a sulfur cathode

Journal:	*Energy & Environmental Science*
Manuscript ID	EE-ART-07-2015-002367.R3
Article Type:	Paper
Date Submitted by the Author:	11-Nov-2015
Complete List of Authors:	Bucur, Claudiu; Toyota Research Institute of North America, Materials Research Department Muldoon, John; Toyota Research Institute of North America, Materials Research Dept. Lita, Adrian; Toyota Research Institute of North America, Materials Research Department

A layer-by-layer supramolecular structure for a sulfur cathode

Claudiu B. Bucur, John Muldoon* and Adrian Lita

Toyota Research Institute of North America, 1555 Woodridge Avenue, Ann Arbor, MI 48105, USA

*Correspondence to: john.muldoon@tema.toyota.com, (734) 995-4403

Ordered, supramolecular structures which aim at tailoring the surface properties of materials have been greatly influenced by the advent of the layer-by-layer (LBL) self-assembly techniques. Any material with bonding abilities (ionic or hydrogen bonds) and which is accessible by a solvent can be transformed by assembly into a multilayer by the LBL approach. Here we propose a nanostructured sulfur cathode with a truffle-like architecture which comprises a sulfur particle embedded with hollow carbon nanospheres and encapsulated with an ion-selective, flexible LBL nanomembrane decorated with conductive carbon. As a result of this hierarchical arrangement cathodes with a final loading of 65% sulfur can operate at a high rate of 2C (a 1C rate corresponds to a complete charge or discharge in 1 hour) for over 500 cycles with nearly 100% coulombic efficiency. These results indicate that this type of nanointerfacial engineering could also be a promising solution for the low electrical conductivity of other battery cathodes.

Broader context: One of the most far-reaching electrochemical successes in recent years has been the development and commercialization of the lithium ion battery which has changed the world in numerous ways. Lithium ion batteries now power cell phones, portable computers, power tools and electric drive vehicles. However, consumer desire for cell phones that last longer and lower cost EVs that drive further fuel an on-going thirst for higher energy batteries. This quest attracts interest towards enhancing the volumetric energy density of lithium ion batteries and towards finding a post lithium ion battery with 2-3 times the energy density of what lithium ion can offer. The banner of post lithium ion battery research is carried by lithium/sulfur, lithium/air and multivalent metal batteries. Here we demonstrate a nanostructured sulfur cathode with a truffle-like architecture which comprises a sulfur particle embedded with hollow carbon nanospheres and encapsulated with an ion-selective, flexible layer by layer nanomembrane decorated with conductive carbon to enhance the performance of lithium – sulfur batteries.

TOC:

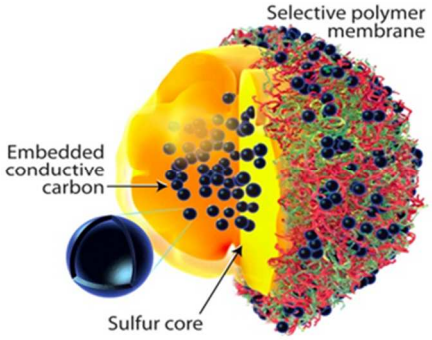

Introduction

The most influential area of polymer thin films is the alternating adsorption of oppositely charged polyelectrolytes popularized by the introduction of the layer-by-layer (LBL) self-assembly technique. In this field, ordered, supramolecular structures aim at tailoring surface properties of materials which govern their applications. The LBL method permits the fabrication of multilayererd thin films on solid supports by the self-limiting adsorption of cationic and anionic species with more than the stoichiometric number of charges (relative to the substrate), from dilute aqueous solutions.[1–3] Each adsorbed layer reverses the surface charge. The driving force for the multilayer film buildup is primarily ion exchange between polyelectrolyte counterions and oppositely charged sites on the "partner" polymer backbone. Precise measurements have concluded that these compensation exchanges responsible for assembly are entropic in nature.[4] While the "electrostatic" model is the more popular LBL method of thin film formation, other methods such as based on the hydrogen bond as a driving force were also reported where polymers bearing hydrogen bond donors and acceptors are employed as building blocks for the LBL assembly.[5]

While initial studies employed flat substrates, many current investigations apply the LBL technique to spherical substrates such as colloids and nano/micro particles.[6] Due to the versatility in material selection and the wide availability of building blocks, polyelectrolyte multilayers are promising systems towards the development of microencapsulation technologies with permeation control. These core-shell particles exhibit properties substantially different from those of the template core which makes them attractive to scientists and technologists alike. Due to the ease of aqueous assembly and simple control parameters such as salt concentration or pH, it is without surprise that these smart shells have garnered momentum as promising applications in biological fields such as controlled drug delivery[7,8] or biocompatible surfaces.[9,10] Here we build on this body of knowledge and bridge the gap towards a mechanistic understanding for the use of selective LBL nanomembranes for high rate, high loading lithium-sulfur batteries.

While sulfur has been an attractive cathode for more than 50 years its viability has been hindered by two fundamental challenges which need to be resolved.[11] (1) Enhance the conductivity of elemental sulfur. (Unlike commercial lithium ion cathodes ($LiCoO_2$) which possess a high electronic conductivity and do not require significant addition of conductive additives, sulfur is a good insulator – 1 billion times less conductive than $LiCoO_2$.) (2) Control the diffusion of polysulfide intermediates formed during cycling. (During discharge, sulfur reduces stepwise by forming a series of polysulfide intermediates which are ionic in nature and solvate easily in the electrolyte. This causes mass loss of active material upon cycling.) Even

today, while approaches mitigate these fundamental challenges of low conductivity and dissolution of polysulfides, they also diminish the superior charge capacity of sulfur.[12–18] One problem deriving from the insulating nature of sulfur is the need for high loadings of conductive additives to improve the overall electronic conductivity. This results in low sulfur content in the cathode. A second problem is the slow rate of operation due to the low electronic conductivity of sulfur and the low ionic conductivity of the reduced product, Li_2S. Third, the diffusion of ionic polysulfides limits cycle life due to anode passivation and mass loss from the cathode.

Extensive research efforts have been devoted to developing methods to address these problems using sulfur infusion into conductive hosts or polymer coatings of sulfur composites.[14,19–21] Since the pioneering findings by Nazar[14] who demonstrated the benefit of infusing sulfur into ordered mesoporous carbon, various micro/nano carbon hosts including spheres, nanofibers, graphene oxide and carbon paper have been investigated as conductive hosts to contain the sulfur active material. Manthiram has recently demonstrated a microporous carbon interlayer with pore sizes matching the dimensions of the polysulfide ions.[22] Tarascon infused sulfur into metal organic frameworks (MOF) with hopes of benefiting from interactions between the polysulfides and the MOF oxide surface.[13] While these approaches improve the conductivity of the sulfur cathode, they are still plagued by diffusion of polysulfides out of the host pores which limits cycle life. Furthermore, the overall sulfur loading in the electrode is low.

Polymer coatings have also been explored to encapsulate and confine elemental sulfur or sulfur composites by providing thin barriers to the migration of the polysulfide intermediates.[23–31] Notable examples include the work of Cui who reported a polymer encapsulated hollow sulfur nanosphere cathode.[27] The empty space inside the sphere allowed expansion inwards without rupturing the rigid polymer coating during discharge. Recently, Manthiram described the use of a mixed ionic electronic conductor (MIEC) consisting of electronically conductive polypyrrole and a polyelectrolyte.[32] He demonstrated that the MIEC inhibits the dissolution of polysulfide ions without disrupting lithium ion transport. While thin polymer coatings do not impede the conductivity of the electrode, they are not optimal barriers against polysulfide migration. Consequently, thicker coatings are more successful at impeding the loss of polysulfides but increase the resistance of the electrode. Inspired by the work of Cui and Manthiram, Muldoon suggested the use of a thin selective nanomembrane assembled by sequential adsorption of oppositely charged polyelectrolytes which provides uniform encapsulation.[24] Controlling the electrode nanostructure is the key to improving the cycle life and rate performance of a sulfur cathode and is still an ongoing challenge.

We demonstrate a sulfur particle embedded with hollow carbon nanospheres which is encapsulated by conductive nanomembranes (Fig. 1). Such architecture which emulates a hazelnut chocolate truffle has multiple advantages: (A) the hollow carbon embedded inside the sulfur core promotes electronic conductivity and sulfur utilization while minimizing the addition of conductive carbon in the electrode. (B) the hollow space inside the carbon structures can accumulate polysulfides and reduce outwards expansion during discharge. (C) the ion-selective nanomembrane impedes the escape of polysulfides while permitting the diffusion of lithium ions (D) nanocarbon is also decorating the membrane to promote conductivity and minimize the carbon loading. This nanoarchitecture overcomes the dilemma associated with maximizing the sulfur loading without compromising the electrical conductivity and retention of polysulfides.

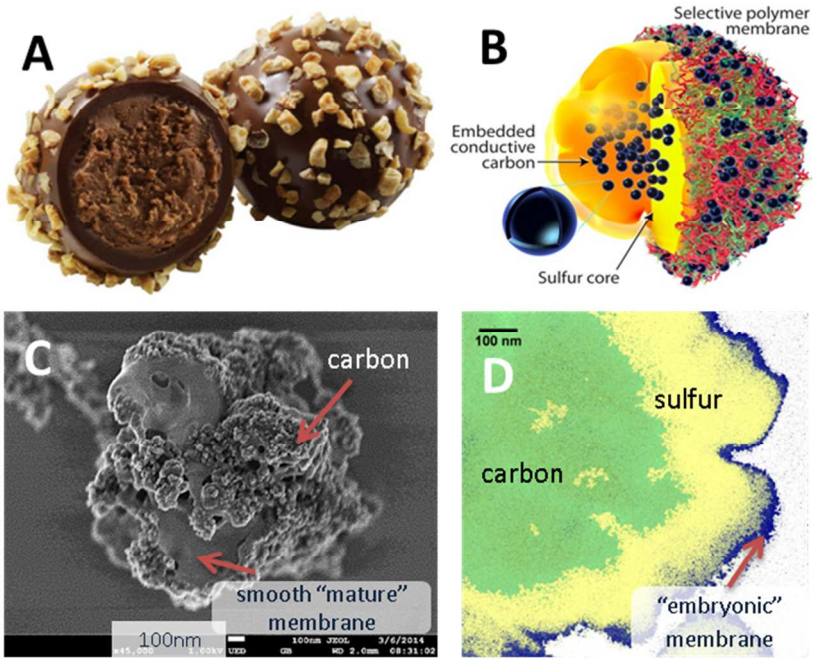

Figure 1 | Schematic of truffle inspired design. Picture of Godiva truffle (A) – our inspiration and a three-dimensional view of our concept (B) depicting the carbon infused sulfur core, the hollow carbon nanoparticles and the multilayer selective polymer membrane decorated with functionalized carbon. The carbon infused into the sulfur core increases sulfur utilization and conductivity allowing for high rates of operation and high, sustainable capacities. The hollow space inside the sulfur core allows for internal volume expansion by polysulfide migration. The sulfur core also contains hollow domains which serve the same purpose as seen in Supplementary Fig. S1. The multilayer polymer membrane serves two functions: 1) reinforces the initial polymer coating (this "embryonic" coating often ruptures due gas evolution during in situ preparation of particles as seen in Supplementary Fig. S1; 2) provides selectivity between diffusion of polysulfides and lithium ions (see Fig. 3). The carbon decoration of this outer membrane provides intimate contact with the polymer membrane which results in increased electronic conductivity and reduced the carbon loading in the cathode. An SEM image (C) depicts the typical outer surface of a sulfur particle containing the selective "mature" polymer membrane and carbon decoration. A TEM/EELS analysis (D) depicting the embedded carbon (green) the sulfur core (yellow) and the initial ("embryonic") polymer coating of a sulfur particle (blue). The outer selective membrane and carbon decoration were omitted for clarity.

Experimental

Sulfur Particle Synthesis. Functionalized (overall negative charge by means of –COOH) Ketjen black 600jd/SuperPLi carbon was prepared by stirring 200 mg carbon in a 0.5 liter mixture of 375 ml H_2SO_4 (90%), 125 ml HNO_3 (33%) under reflux for 2 hours (70˚C). PVP-sulfur nanoparticles were prepared by mixing 25 ml concentrated HCl (37%) with a solution containing 20g $Na_2S_2O_3$ and 12g PVP to a total volume of 0.5L deionized water. As illustrated in Fig. 2A, PEDOT:PSS-sulfur nanoparticles were prepared by the mixing of 25 ml concentrated HCl (37%) with a solution containing 20g $Na_2S_2O_3$ and 7 ml PEDOT:PSS (1% conductive grade solution in water from Sigma Aldrich). PVP-sulfur nanoparticles incorporating hollow carbon were prepared by the addition of a solution comprised of 90

mg functionalized Ketjen Black 600jd sonicated in 25 ml concentrated HCl (37%) to a solution containing 20g $Na_2S_2O_3$ and 12g PVP in a total volume of 0.5L deionized water. The size and shape of the sulfur particles can be modified by varying the polymer concentration and mixing regimes, as depicted in Supplementary Fig. S3. As illustrated in Fig. 2K, PEDOT:PSS-sulfur nanoparticles incorporating hollow carbon were prepared by the addition of a solution comprised of 75 mg functionalized Ketjen Black 600jd sonicated in 25 ml concentrated HCl (37%) to a solution containing 20g $Na_2S_2O_3$ and 7ml PEDOT:PSS (1% conductive grade solution in water from Sigma Aldrich) in a total volume of 0.5L deionized water. On this PEDOT:PSS-sulfur foundation, five polymer layers (positively charged PDADMAC and the complementary negatively charged PEDOT:PSS) were adsorbed sequentially by exposure to dilute aqueous (0.1M) solutions of oppositely charged polyions with a 0.1M ionic strengths of lithium nitrate. A rinse step was always employed to clean the carbon/sulfur particle of any loosely bound polymer chains and ensure homogeneous coverage. A 1L custom filtration apparatus (1.0 μm pore size) from Ace Glass was used for the membrane assembly. Functionalized (negatively charged) SuperPLi particles were adsorbed onto the last PDADMA polymer layer from a well sonicated solution of 300 mg carbon in 0.5L deionized water. This active material was dried under vacuum at 60 ˚C overnight. TGA experiments revealed 85% sulfur loading (Supplementary Fig. S4). Similarly, on a PVP-sulfur foundation the following layers were adsorbed (0.1M polymer solutions, 300mg SuperpLi per 0.5L deionized water): PAA/PEO/PAA/PVP/PAA/PEO/SuperpLi at pH2. The low pH is required for the last step to assure that the –COOH functionalization of SuperpLi remains protonated and H-bonds with the oxygen on PEO. This active material was dried under vacuum at 60 ˚C overnight. TGA experiments revealed 82% sulfur loading (Supplementary Fig. S4).

Electrochemistry. The battery performance was evaluated by galvanostatic cycling of coin cells with the sulfur truffle cathodes as the working electrode and lithium foil as the counter/reference electrode. The working electrodes were prepared by the typical slurry method (70 μm thick by doctor blade) with sulfur truffle powders, Ketjen Black 600jd carbon and SBR/CMC (1:1 by weight) binder with a mass ratio of 80:15:5 (H-bonded PVP based truffle cathode) and 60:35:5 (ion exchange PEDOT:PSS based truffle) and water/ethanol (typically 1:1). The electrodes were dried under vacuum at 60 ˚C for 24 hours and then transferred inside the Ar filled box for coin cell assembly. The electrode was punched into disks with a 0.785 cm^2 area for cell assembly. The areal mass loading of sulfur was 1 – 1.5 mg/cm^2. The electrolyte contained 1M LiTFSI, 0.5M $LiNO_3$ and 0.04M $CsNO_3$ and 10% of a concentrated lithium polysulfide solution in DOL(dioxolane):DME(glyme):hexane 48:48:4. Preliminary work (Supplementary figures S5 and S6) suggests that small amounts of hexane and polysulfides added to the electrolyte result in improved capacity and a reduced overcharge. A recent paper details a possible explanation for the function of the polysulfides.[33] The polysulfide capacity of the electrolyte has been measured independently of the sulfur cathode and is less than 0.05% of the typical cathode capacity reported. The concentrated lithium polysulfide solution was prepared from the reaction of lithium metal and elemental sulfur in stoichiometric ratios at a temperature of 60 ˚C, in DOL:DME (1:1 mixture). After 1 week, the solution was filtered and mixed with lithium salts as described above. 2032 stainless steel coin cells with one Celgard 2325 separator were used for electrochemical measurements. One drop of electrolyte (<20 microliters) was dispensed per cell. Charge and discharge rates were calculated assuming theoretical capacity for the total amount of sulfur in the cathode. BioLogic SAS, model VMP3, multi-channel Science Instruments potentiostats were used for electrochemical measurements. Data were processed with EC-Lab Software V10.35 with the corresponding VMP3 firmware, provided by Science Instruments.

SEM: Sulfur truffle particles were dispersed in water by sonication. Upon dilution a drop was dispensed on a clean silicon wafer which was kept under vacuum, at 60 °C for 12 hours. Images were obtained with a field-emission SEM (JOEL JSM-6700F) at 1 kV (gentle beam conditions).

TEM/EELS: Samples were prepared by drop drying sulfur truffle ethanol suspensions onto carbon lacey TEM grids (EMS, 200 mesh). A cryo-probe sample holder was used to protect the sample from electron-beam damage. HRTEM images and EEL spectra were collected on an FEI Titan Krios

TEM equipped with a cold field-emission electron source, operating with a probe current of 75 μA and an accelerating voltage of 300 kV. EEL spectra were collected using a Gatan GIF Tridiem 863 spectrometer with an EELS collection semi-angle of 120 mrad. 20 eV width spectra centered on the standard edge for each element were collected. A complete energy loss spectrum was recorded for each pixel on the EELS image. From this image an elemental map was constructed as follows: (1) background subtraction (2) noise filtering and (3) color coding summation of the resulting pixels.

Results and Discussions

We used a simple, scalable, room temperature bottom up approach tailored to the coating, filtering, rinsing and recoating of truffle sulfur nanoparticles ranging in diameter from 200nm to 700nm. Polydispersity is desirable for electrode materials to increase tap density. Sulfur nanoparticles were obtained based on a simple reaction between sodium thiosulfate and hydrochloric acid in an aqueous solution in the presence of polymers at room temperature. It should be noted that polymer coated sulfur particles were similarly reported by Cui.[27] However, the reported approach is lacking a mechanism for controlling the thickness or the permeability of adsorbed polymer at the nano level. The weakly adsorbed polymer capsule can dissolve in electrolyte over time, effectively dismantling the capsule. In addition, it is desirable to graft a conductive polymer directly onto the insulating surface of the sulfur particle. In this simplified demonstration we show a conductive grade poly(3,4-ethylenedioxythiophene): polystyrene sulfonate (PEDOT:PSS) encapsulating a sulfur particle (Fig. 2A) The hydrophobic domains of this polymer favor the growth of elemental sulfur while the hydrophilic domains solvate well in the aqueous solution. Such antagonistic effect gives rise to polymer encapsulated sulfur nanospheres. Figure 2B shows typical scanning electron microscopy (SEM) images of the PEDOT:PSS encapsulated sulfur nanoparticles. A key feature easy to identify is the polydispersed particle size ranging in diameter from 200nm to 700 nm. Well rinsed, the thin conductive PEDOT:PSS polymer coating serves as the foundation on which additional polymer layers can be adsorbed with the layer by layer technique. This “embryonic membrane” is electronically conductive and allows for easy electrolyte access to the sulfur core but it is not yet thick and elastic enough to accommodate volume changes which occur during reversible transitions from S_8 to Li_2S. Also, since it is composed of a thinly adsorbed single polymer, it does not possess a mechanism for selectively impeding polysulfide migration. However, a fully selective (mature) membrane can be assembled on top of the PEDOT:PSS foundation when this primary structure is sequentially exposed to aqueous solutions of oppositely charged polyelectrolytes (Supplementary figure S7A – ellipsometric thickness measurement of membrane assembly on a surrogate silicon wafer and figure S7B – zeta potential measurements of surface charge alternation during LBL adsorption of polymer layers onto the primordial sulfur particle). While most charged monomer units on the polymer backbone exchange their counterions and pair up to “crosslink” the membrane, a few monomer units will retain their original small ion partners. It has been reported that a diffusing ionic species can now pair exchange with these small counterions and have a migration path through the membrane (Fig. 3B).[34] These “defects” govern properties such as membrane growth, permeability and selectivity as well as membrane elasticity.[35,36] Several layers are usually needed to fully encapsulate the sulfur substrate. SEM imaging of drop casted suspensions (Supplementary Fig. S2A) show spherical particles with a relatively smooth surface. Transmission electron microscopy (TEM) also shows a homogeneous internal structure (the sulfur core) (Fig. S2B).Once assembled, the mature membrane exhibits selective ionic conductivity. Monovalent lithium salts can easily

penetrate the membrane while divalent, bulkier polysulfide salts migrate exponentially slower. In order to cross the membrane, divalent polysulfides require the simultaneous displacement of counterions from 2 adjacent "defects" as opposed to just 1 for the lithium salts. The mechanism for the selectivity of LBL membranes to the valence number of the diffusing species has been previously detailed.[36] In an attempt to enhance the electronic conductivity of the ionic selective membrane 50 nm carbon nanospheres were functionalized to possess an overall negative charge and decorated the outer positively charged membrane layer (Fig. 2F). The carbon decoration can be observed by backscatter filtered SEM in Fig. 2G.

There are two interdependent characteristics of this nano-design that enable superior battery performance. The first is a hierarchical architecture of the selective membrane which severely depresses the diffusion of polysulfides. Assembly of the membrane can be achieved based on the ion exchange principle (where charged moieties on the polyelectrolyte backbone exchange their small solution counterions with oppositely charged moieties of the complementary polyelectrolyte) or on hydrogen bonding (typically H-O bonds where the hydrogen and oxygen reside on complementary polymers). It should be noted that recent studies have shown that layer by layer assembled multilayer membranes can repair damage such as cracks and cuts in the presence of solvent.[37] The second characteristic is very low loadings of conductive carbon additive in the composite. In this architecture, as little as 5% carbon in the membrane can activate 93% sulfur (the remainder 2% can be allocated to the polymer used). However, it is challenging to transport electrons inside the sulfur core with the goal of increasing sulfur utilization. Our approach was to incorporate hollow carbon nanospheres early during the sulfur particle synthesis (Fig. 2K, S2D). SEM imaging (Fig. S2C) shows a spherical surface marked by deep invaginations. TEM (Fig. S2D) shows a sulfur core with a complex consistency in line with the presence of the hollow carbon nanospheres. It is worth noting that the large surface grooves and the inhomogeneous internal consistency observed here is clearly in contrast with the smooth surface and homogeneous core from Fig. S2A and S2B which are associated with sulfur particles which do not incorporate hollow carbon particles. EELS/TEM mapping of the carbon (green) embedded sulfur core (yellow) is presented in Fig. 1D. The empty void space introduced in the sulfur core can accumulate polysulfide reduction products and reduce the stress on the encapsulating membrane by minimizing outwards expansion during cycling.

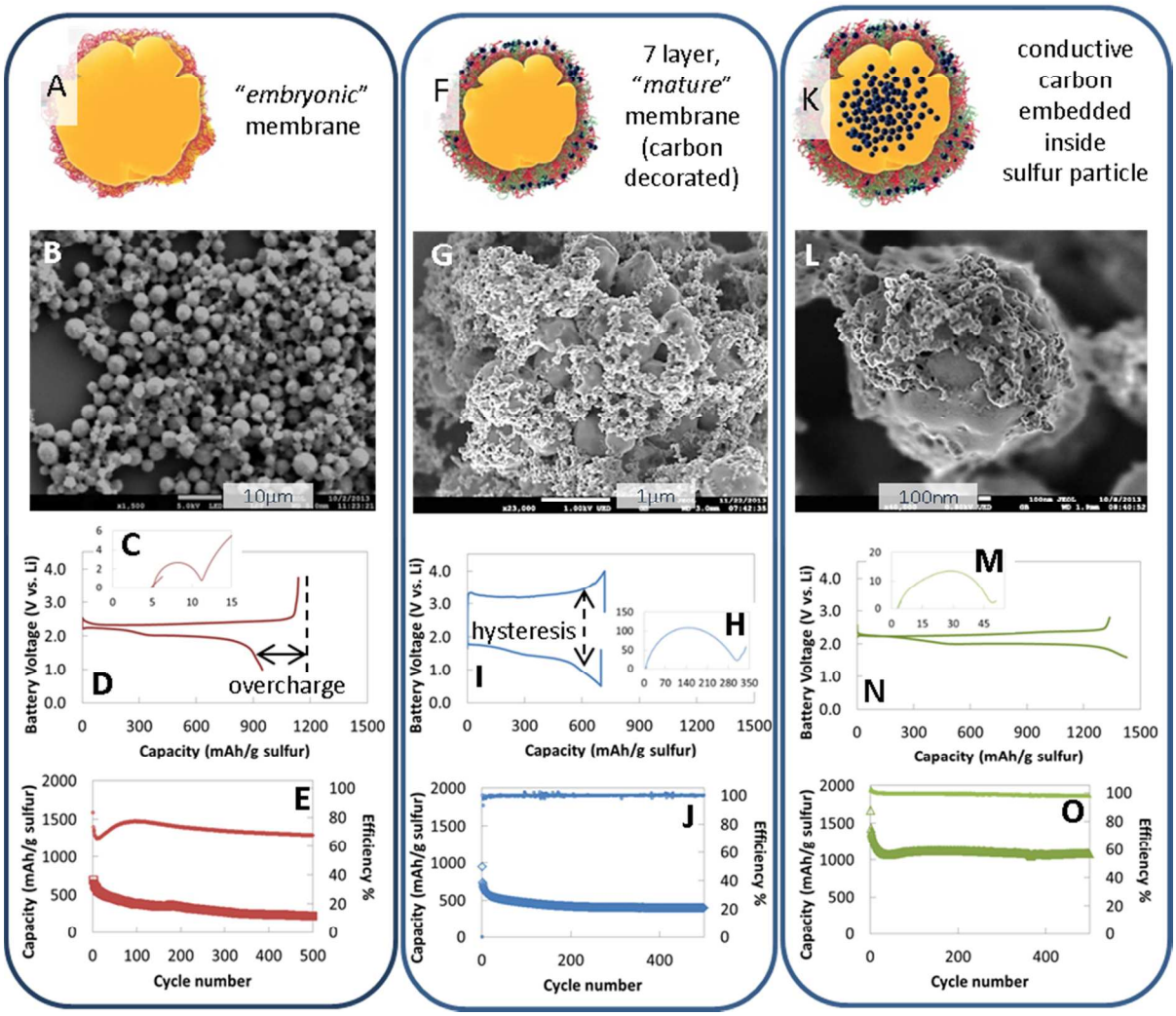

Figure 2 | Fabrication, imaging and electrochemical characterization of sulfur cathodes. For the purpose of depicting the relationship between the architectural design of the sulfur particle and the electrochemical operation of cathodes containing it, we display three types of sulfur nanocomposites with sulfur loadings of ~1 mg/cm^2 and ~50% by mass in the finished cathode. However, higher sulfur loadings can be achieved and are presented in Fig. 4. All battery cycling was performed at a fast rate of 2C (charge/discharge in 30 minutes). Impedance units are Ω·cm. (A) illustration depicting a sulfur particles stabilized by a PEDOT:PSS polymer "embryonic" membrane. A "mature" membrane is not yet assembled. Notice that this particle does not contain embedded conductive carbon; (B) SEM image of drop-casted sulfur particles on a silicon wafer; (C) cell impedance of a sulfur cathode prepared from sulfur particles described in (A) before cycling. Note the low impedance afforded by the thin "embryonic" membrane; (D) the first fixed current charge/discharge electrochemical profile of a sulfur cathode prepared from sulfur particles described in (A). Note the overcharge due to the inability of the "embryonic" membrane to stop the loss of polysulfides; (E) capacity fade over the first 500 cycles for a cathode comprised of (A); (F) illustration depicting a 7 layer (PEDOT:PSS/PDADMAC) "mature" membrane assembled onto the foundation offered by the "embryonic" membrane from illustration (A). In order to improve its electronic conductivity, the "mature" membrane is decorated with functionalized, conductive carbon; (G) SEM figure of an aggregation of sulfur

particles described in illustration (F); (H) cell impedance of (F) before cycling. Note the increase in impedance (compared to (C)) presumably due to the increase in impedance caused by assembly of the "mature" membrane (I) the first fixed current charge/discharge electrochemical response for (F). Notice the addition of the "mature" membrane removes overcharge presumably by inhibiting polysulfide dissolution but it ads considerable hysteresis between charge and discharge plateaus. (J) capacity fade over the first 500 cycles for a cathode prepared from (F). (K) illustration depicting sulfur particles synthesized in a dispersion of functionalized conductive carbon. The results is the embedding of conductive carbon inside the sulfur particle which is then sequentially coated by a "mature" membrane and again decorated with conductive carbon similar to illustration (F); (L) SEM image of a sulfur particles on a silicon wafer. Notice the conductive carbon decorating the smooth membrane particle surface. TEM images depicting the presence of carbon inside the sulfur particles are shown in figures 1D and S2; (M) cell impedance of (K) before cycling. Notice the reduction of impedance (if compared to (H)) presumably due to the embedding of conductive carbon inside the sulfur particle; (N) the first fixed current charge/discharge electrochemical profile for (K). Notice that while the lack of overcharge is maintained (the "mature" membrane has been utilized here), the hysteresis between charge and discharge plateaus is also reduced to acceptable levels (if compared to (I)) possibly due to the embedding of conductive carbon inside the sulfur particle; (T) capacity fade over the first 500 cycles for a cathode assembled from (K).

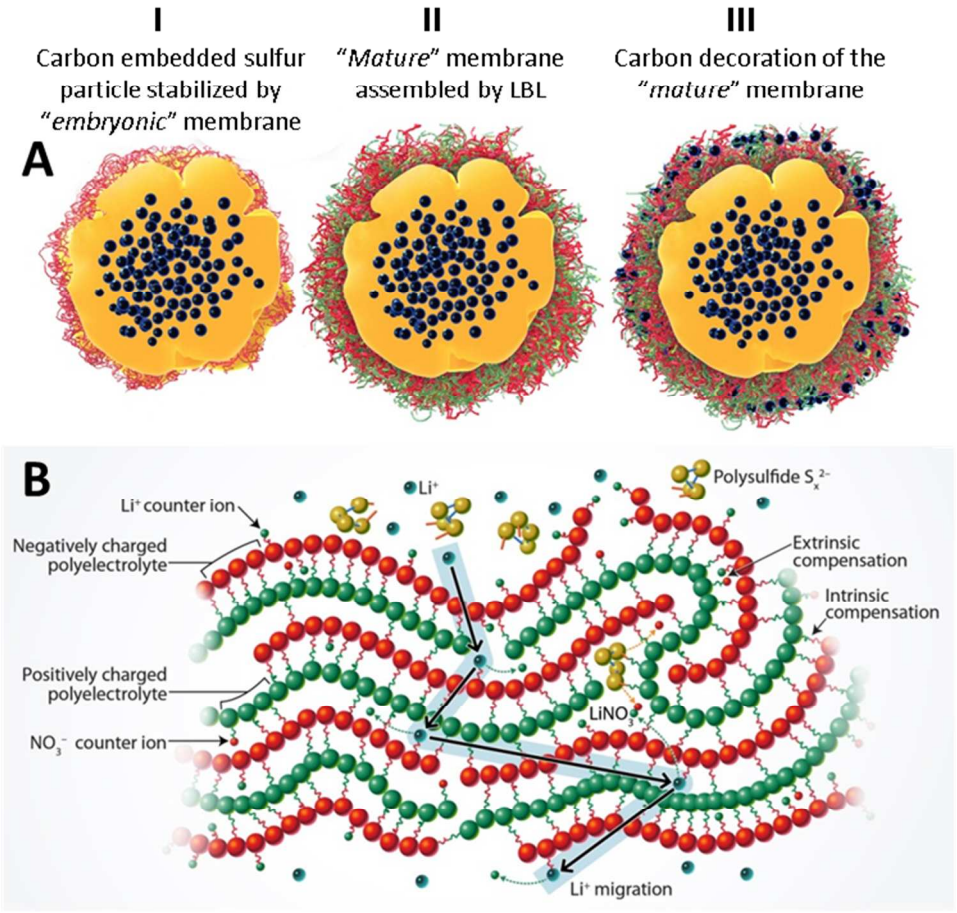

Figure 3 | Tuning the sulfur particle encapsulating membrane – the mechanism behind the membrane's selectivity. (A) Due to incomplete coverage of the sulfur core by the initial, "embryonic" membrane (I), 7 additional polymer layers were adsorbed to provide a homogeneous yet thin barrier to polysulfides (II). This LBL "mature" membrane was then decorated with functionalized carbon for increase conductivity and a reduction of the overall carbon content of the cathode (III). The typical decoration coverage is depicted by SEM in Fig. 1C and 2L. Excess decoration is possible and depicted in Supplementary Fig. S8. This process is depicted schematically in panel A. Polymer layers adsorb sequentially due to ion exchange between oppositely charged polymers; (B) Diffusion of charged species through a LBL membrane is well understood and has been previously reported. *Intrinsic sites* form when two oppositely charged polymers crosslink electrostatically by expulsion of their original counterions in the mixing solution. It is the *intrinsic sites* which hold the membrane together. However, a small percentage of the original ions will not leave their polymeric partners and will be incorporated in the membrane as "defects" (the ratio of defects can be tuned during membrane assembly). These defects are called *extrinsic sites* and are responsible for the hopping (by ion exchange) of charged diffusing species such as Li^+ or S_x^{2-}. The larger and divalent polysulfides will spend a longer time diffusing due to the lower chance of finding two extrinsic sites close enough to ion exchange with and migrate out of the truffle, whereas monovalent Li^+ will spend considerably less time hopping between extrinsic sites to move in and out of the sulfur nanocomposite.

It should be noted that many publications only report prolonged cycle life (beyond 200 cycles) at very low rates (0.5C or below). However high rates of operation are desired for high power applications such as electric transportation (vehicles or planes) and robotics. We therefore tested our sulfur cathodes at a very fast rate of 2C (charge or discharge in 30 minutes). Fast battery operation can only be achieved with enhanced electronic conductivity which has been so far difficult to achieve with an insulating active material such as sulfur. In addition, fast battery operation suffers from high hysteresis between charge and discharge voltages and fast capacity decay. Initially, an "embryonic membrane" (Fig. 2A) composed of conductive grade PEDOT:PSS encapsulated a sulfur particle (~500nm diameter). The impedance measurements of the cathode revealed that this material has low interfacial charge transfer resistance (Fig. 2C). While charge/discharge voltage hysteresis is low (~0.5V hysteresis), overcharge is observed (which lowers the coulombic efficiency) and corresponds to loss of polysulfides (Fig. 2D). This embryonic membrane often ruptures due to gas evolved during the in situ formation of sulfur (Supplementary Fig. S1). This translates into 80% capacity fade over 500 cycles (150 mAh/g sulfur at cycle 500). The coulombic efficiency stabilizes at 70% (Fig. 2E). To impede the migration of polysulfides, a 7 layer "mature membrane" was assembled by sequential absorption of poly diallyldimethylammonium chloride (PDADMAC) and PEDOT:PSS. In an effort to enhance its electrical conductivity, the membrane was decorated with 50nm conductive carbon (Fig. 2F). As a result, no overcharge was observed and the coulombic efficiency was stable at 100% for over 500 cycles. Capacity fade was reduced to a 33% loss (500 mAh/g sulfur at cycle 500). While the coulombic efficiency of 100% suggests that the membrane impedes polysulfide migration better than the PEDOT:PSS coating, only 1/3 of the active sulfur is utilized based on capacity. This low sulfur utilization is supported by an impedance 20 times greater (Fig. 2H). In addition, the hysteresis between the charge and discharge plateaus increased three fold to ~1.5V

(Fig. 2I-J). It is desirable to minimize the voltage hysteresis between charge and discharge plateaus for high charging energy efficiency as well as increase the utilization of active sulfur.

Indeed, the cathode remains stable throughout battery cycling (Supplementary Fig.S9) and affords remarkable battery performance. To overcome the challenge of low electrical conductivity and sulfur utilization the nano-design described above was complemented by the early incorporation of hollow carbon nanospheres into the sulfur particle early during synthesis (Fig. 2K, S2D). The addition of hollow carbon into the sulfur core decreased the impedance by a factor of 6 which resulted in a very low voltage hysteresis between charge and discharge (~0.25V). In addition, the sulfur utilization is doubled. Stable capacities of 1000 mAh/g sulfur are obtained after 500 cycles, compared to 150 mAh/g sulfur obtained for a single PEDOT:PSS layer coated sulfur particle. The coulombic efficiency was stable at 100% (Fig. 2N-O). It is interesting to note the concern of self-discharge or overcharge when slow rates are applied. When the cycling of this sulfur truffle cathode was interrupted for 2 days, no loss in capacity was observed when the cycling was resumed (Supplementary Fig. S10). Cycling at 0.5C and 5C is shown in Supplementary Fig. S11.

In addition to ion exchange, another assembly approach for building a multilayer membrane is through hydrogen bond interactions between distinct polymers. Building on the groundbreaking work of Cui who used a coating of polyvinylpyrrolidone (PVP) to form hollow sulfur nanoparticles,[27] we utilized hydrogen bonding to assemble a multilayer membrane using PVP as the foundation polymer layer. Subsequent layers consisted of neutral polymers previously reported as components of sulfur cathodes such as polyacrylic acid (PAA) and polyethylene oxide (PEO). We maintained the architecture by incorporating hollow carbon during the sulfur particle formation and decorating the membrane exterior. This approach resulted in a dramatic enhancement in the rate of operation of the sulfur cell compared to the work of Cui who reports a capacity of 700 mAh/g sulfur after 500 cycles at a rate of C/2 with a cathode sulfur loading of 50%. Our truffle architecture affords a C rate 4 times faster (2C) and a 30% higher sulfur loading (65%) in the cathode. The capacity observed after 500 cycles is 750 mAh/g sulfur (Fig. 4). No overcharge is observed and the cathode impedance is low. This remarkable battery performance clearly indicates that this type of nanointerfacial engineering is crucial for solving the problem of low electrical conductivity and polysulfide dissolution of sulfur cathodes.

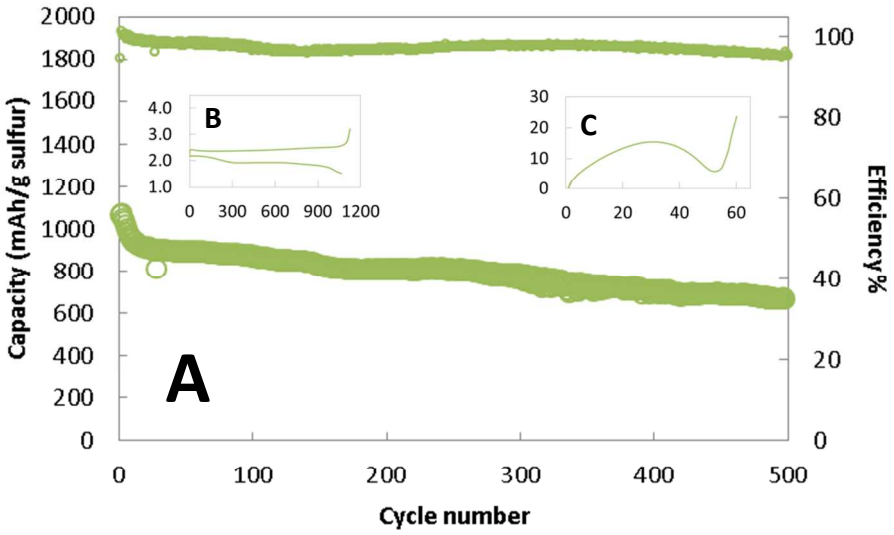

Figure 4 | (A) Capacity fade over the first 500 cycles for batteries with optimized truffle sulfur cathodes containing particles encapsulated by a 7 layer polymer membrane (PVP/PAA/PEO). Batteries consist of 2032 coin cells with a sulfur loading of ~1 mg/cm^2 and ~65% sulfur loading by mass in the finished cathode. All battery cycling was performed at a fast rate of 2C. Insets display the first fixed current charge/discharge profile (B) as well as impedance before cycling (C).

Conclusion

In summary, we have developed a nano-architecture which enhances the electrical conductivity and impedes dissolution of sulfur polysulfides. This is achieved by the incorporation of conductive carbon inside sulfur particles which are sequentially wrapped with ion selective LBL nano-membranes. The synthesis is both simple and modular. We believe that this nanoengineering may lead to a viable route towards a high energy density battery with a sulfur cathode. This proof of concept of a self-healing, conductive membrane may have further reaching applications beyond lithium-sulfur, such as silicon or tin anodes, where the self-healing nature of the membrane may overcome the volumetric changes during the lithiation/delithiation of the alloy anodes.

References:

1 G. Decher, *Science*, 1997, **277**, 1232–1237.
2 F. Caruso, R. A. Caruso and H. Möhwald, *Science*, 1998, **282**, 1111–1114.
3 H. Ejima, J. J. Richardson, K. Liang, J. P. Best, M. P. van Koeverden, G. K. Such, J. Cui and F. Caruso, *Science*, 2013, **341**, 154–157.
4 C. B. Bucur, Z. Sui and J. B. Schlenoff, *J. Am. Chem. Soc.*, 2006, **128**, 13690–13691.
5 G. Wu and X. Zhang, in *Multilayer Thin Films*, eds. G. Decher and J. B. Schlenoff, Wiley-VCH Verlag GmbH & Co. KGaA, 2012, pp. 43–67.

6 F. Caruso, H. Lichtenfeld, M. Giersig and H. Möhwald, *J. Am. Chem. Soc.*, 1998, **120**, 8523–8524.
7 B. G. De Geest and S. C. De Smedt, in *Multilayer Thin Films*, eds. G. Decher and J. B. Schlenoff, Wiley-VCH Verlag GmbH & Co. KGaA, 2012, pp. 749–763.
8 J. Fei, Y. Cui, Q. He and J. Li, in *Multilayer Thin Films*, eds. G. Decher and J. B. Schlenoff, Wiley-VCH Verlag GmbH & Co. KGaA, 2012, pp. 777–799.
9 A. P. R. Johnston, G. K. Such, S. J. Dodds and F. Caruso, in *Multilayer Thin Films*, eds. G. Decher and J. B. Schlenoff, Wiley-VCH Verlag GmbH & Co. KGaA, 2012, pp. 801–829.
10 I. Lee, in *Multilayer Thin Films*, eds. G. Decher and J. B. Schlenoff, Wiley-VCH Verlag GmbH & Co. KGaA, 2012, pp. 985–1001.
11 A. Manthiram, Y. Fu, S.-H. Chung, C. Zu and Y.-S. Su, *Chem. Rev.*, 2014, **114**, 11751–11787.
12 H. Yao, G. Zheng, P.-C. Hsu, D. Kong, J. J. Cha, W. Li, Z. W. Seh, M. T. McDowell, K. Yan, Z. Liang, V. K. Narasimhan and Y. Cui, *Nat. Commun.*, 2014, **5**.
13 R. Demir-Cakan, M. Morcrette, F. Nouar, C. Davoisne, T. Devic, D. Gonbeau, R. Dominko, C. Serre, G. Férey and J.-M. Tarascon, *J. Am. Chem. Soc.*, 2011, **133**, 16154–16160.
14 X. Ji, K. T. Lee and L. F. Nazar, *Nat. Mater.*, 2009, **8**, 500–506.
15 M.-K. Song, Y. Zhang and E. J. Cairns, *Nano Lett.*, 2013, **13**, 5891–5899.
16 J. Guo, Y. Xu and C. Wang, *Nano Lett.*, 2011, **11**, 4288–4294.
17 N. Jayaprakash, J. Shen, S. S. Moganty, A. Corona and L. A. Archer, *Angew. Chem. Int. Ed.*, 2011, **50**, 5904–5908.
18 X. Ji, S. Evers, R. Black and L. F. Nazar, *Nat. Commun.*, 2011, **2**, 325.
19 J. Guo, Z. Yang, Y. Yu, H. D. Abruña and L. A. Archer, *J. Am. Chem. Soc.*, 2013, **135**, 763–767.
20 W. Zhou, Y. Yu, H. Chen, F. J. DiSalvo and H. D. Abruña, *J. Am. Chem. Soc.*, 2013, **135**, 16736–16743.
21 K. T. Lee, R. Black, T. Yim, X. Ji and L. F. Nazar, *Adv. Energy Mater.*, 2012, **2**, 1490–1496.
22 Y.-S. Su and A. Manthiram, *Nat. Commun.*, 2012, **3**, 1166.
23 L. Yin, J. Wang, J. Yang and Y. Nuli, *J. Mater. Chem.*, 2011, **21**, 6807–6810.
24 C. B. Bucur, J. Muldoon, A. Lita, J. B. Schlenoff, R. A. Ghostine, S. Dietz and G. Allred, *Energy Environ. Sci.*, 2013, **6**, 3286–3290.
25 H. Wang, Y. Yang, Y. Liang, J. T. Robinson, Y. Li, A. Jackson, Y. Cui and H. Dai, *Nano Lett.*, 2011, **11**, 2644–2647.
26 L. Wang, D. Wang, F. Zhang and J. Jin, *Nano Lett.*, 2013, **13**, 4206–4211.
27 W. Li, G. Zheng, Y. Yang, Z. W. Seh, N. Liu and Y. Cui, *Proc. Natl. Acad. Sci.*, 2013, 201220992.
28 W. Li, Q. Zhang, G. Zheng, Z. W. Seh, H. Yao and Y. Cui, *Nano Lett.*, 2013, **13**, 5534–5540.
29 L. Xiao, Y. Cao, J. Xiao, B. Schwenzer, M. H. Engelhard, L. V. Saraf, Z. Nie, G. J. Exarhos and J. Liu, *Adv. Mater.*, 2012, **24**, 1176–1181.
30 Y. Fu and A. Manthiram, *J. Phys. Chem. C*, 2012, **116**, 8910–8915.
31 J. Muldoon, C. B. Bucur and T. Gregory, *Chem. Rev.*, 2014.
32 Y. Fu and A. Manthiram, *Chem. Mater.*, 2012, **24**, 3081–3087.
33 W. Li, H. Yao, K. Yan, G. Zheng, Z. Liang, Y.-M. Chiang and Y. Cui, *Nat. Commun.*, 2015, **6**.
34 T. R. Farhat and J. B. Schlenoff, *Langmuir*, 2001, **17**, 1184–1192.
35 R. A. Ghostine and J. B. Schlenoff, *Langmuir*, 2011, **27**, 8241–8247.
36 T. R. Farhat and J. B. Schlenoff, *J. Am. Chem. Soc.*, 2003, **125**, 4627–4636.
37 Y. Li, S. Chen, M. Wu and J. Sun, *Adv. Mater.*, 2012, **24**, 4578–4582.

Supplementary Materials:

Figures S1-S11

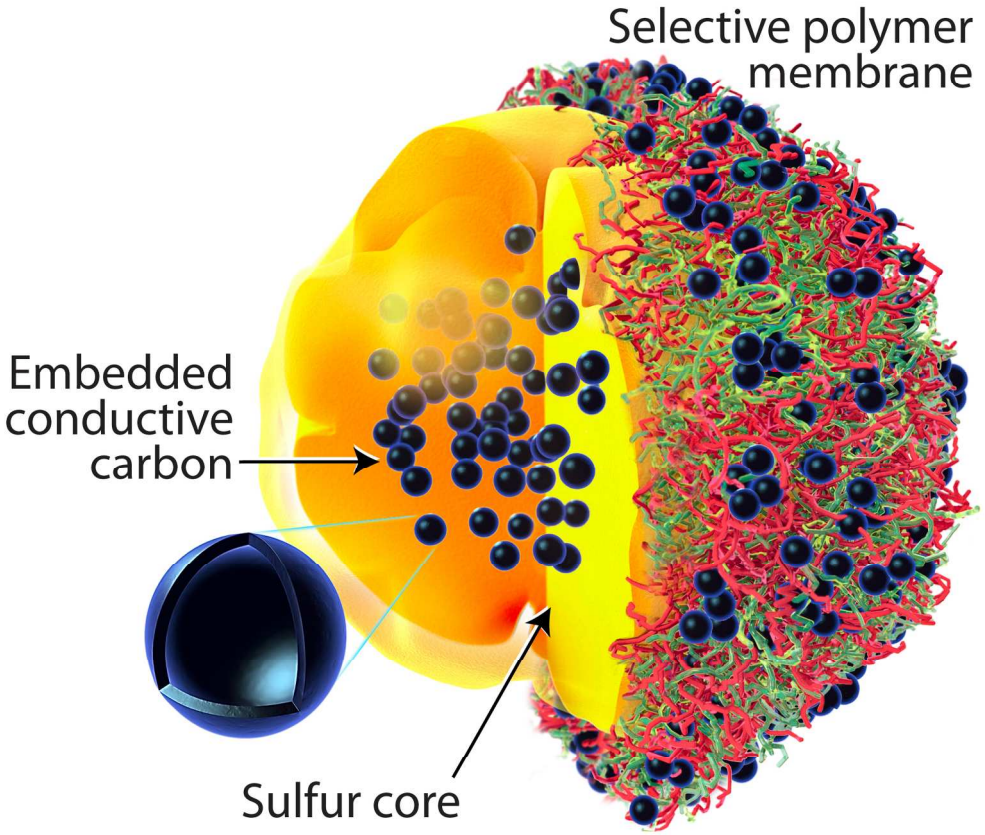

The anatomy of a truffle inspired sulfur particle for a battery cathode
711x614mm (72 x 72 DPI)